2019-12

WAVE ENERGY REFLECTION AT A ROCKY COAST

O'Brien, Kevin J.

Monterey, CA; Naval Postgraduate School

NAVAL POSTGRADUATE SCHOOL

MONTEREY, CALIFORNIA

THESIS

WAVE ENERGY REFLECTION AT A ROCKY COAST

by

Kevin J. O'brien

December 2019

Thesis Advisor:	James H. MacMahan
Second Reader:	Edward B. Thornton

THIS PAGE INTENTIONALLY LEFT BLANK

REPORT DOCUMENTATION PAGE			*Form Approved OMB No. 0704-0188*

1. AGENCY USE ONLY *(Leave blank)*	**2. REPORT DATE** December 2019	**3. REPORT TYPE AND DATES COVERED** Master's thesis

4. TITLE AND SUBTITLE
WAVE ENERGY REFLECTION AT A ROCKY COAST

5. FUNDING NUMBERS

6. AUTHOR(S) Kevin J. O'brien

7. PERFORMING ORGANIZATION NAME(S) AND ADDRESS(ES)
Naval Postgraduate School
Monterey, CA 93943-5000

8. PERFORMING ORGANIZATION REPORT NUMBER

9. SPONSORING / MONITORING AGENCY NAME(S) AND ADDRESS(ES)
N/A

10. SPONSORING / MONITORING AGENCY REPORT NUMBER

11. SUPPLEMENTARY NOTES The views expressed in this thesis are those of the author and do not reflect the official policy or position of the Department of Defense or the U.S. Government.

12a. DISTRIBUTION / AVAILABILITY STATEMENT
Approved for public release. Distribution is unlimited.

12b. DISTRIBUTION CODE
A

13. ABSTRACT (maximum 200 words)

Wave energy reflection, defined as the ratio of offshore to onshore energy flux, R^2, of surface gravity waves from a rough rocky shoreline, was investigated from two individual 15-day Acoustic Doppler Current Profiler (ADCP) deployments at Hopkins Marine Station in Monterey Bay, California. The first was deployed in 9 m water depth, located 100 m seaward of the rocky shoreline, and the second was deployed in 2.5 m water depth, located approximately 6 m from the shoreline. The mean R^2 for both deployments was ~0.08, suggesting minimal reflection. R^2 statistically decreased (at 95% significance) by 0.05 during the transition from low to high tide. R^2 was found to be independent of onshore wave energy. The mean direction of the incoming and outgoing waves was approximately equal and opposite, though the outgoing waves displayed more directional variability. This increase is believed to occur from the alongshore variability of the shoreline that was weakly correlated with tidal elevation. These R^2 are similar to observations at rough coral reefs and breakwaters. It appears that the primary reflector is the shoreline and not scattering by the rough subaqueous bottom. Wave dissipation plays a larger role than wave reflection at this rocky shoreline, which may influence biological community structures and nutrient transport.

14. SUBJECT TERMS reflection, rocky shoreline, bottom friction, dissipation	**15. NUMBER OF PAGES** 43
	16. PRICE CODE

17. SECURITY CLASSIFICATION OF REPORT	**18. SECURITY CLASSIFICATION OF THIS PAGE**	**19. SECURITY CLASSIFICATION OF ABSTRACT**	**20. LIMITATION OF ABSTRACT**
Unclassified	Unclassified	Unclassified	UU

NSN 7540-01-280-5500

Standard Form 298 (Rev. 2-89)
Prescribed by ANSI Std. 239-18

THIS PAGE INTENTIONALLY LEFT BLANK

Approved for public release. Distribution is unlimited.

WAVE ENERGY REFLECTION AT A ROCKY COAST

Kevin J. O'brien
Lieutenant Commander, United States Navy
BS, Temple University, 2009

Submitted in partial fulfillment of the
requirements for the degree of

MASTER OF SCIENCE IN METEOROLOGY AND PHYSICAL OCEANOGRAPHY

from the

NAVAL POSTGRADUATE SCHOOL
December 2019

Approved by: James H. MacMahan
Advisor

Edward B. Thornton
Second Reader

Peter C. Chu
Chair, Department of Oceanography

THIS PAGE INTENTIONALLY LEFT BLANK

ABSTRACT

Wave energy reflection, defined as the ratio of offshore to onshore energy flux, R^2, of surface gravity waves from a rough rocky shoreline, was investigated from two individual 15-day Acoustic Doppler Current Profiler (ADCP) deployments at Hopkins Marine Station in Monterey Bay, California. The first was deployed in 9 m water depth, located 100 m seaward of the rocky shoreline, and the second was deployed in 2.5 m water depth, located approximately 6 m from the shoreline. The mean R^2 for both deployments was ~0.08, suggesting minimal reflection. R^2 statistically decreased (at 95% significance) by 0.05 during the transition from low to high tide. R^2 was found to be independent of onshore wave energy. The mean direction of the incoming and outgoing waves was approximately equal and opposite, though the outgoing waves displayed more directional variability. This increase is believed to occur from the alongshore variability of the shoreline that was weakly correlated with tidal elevation. These R^2 are similar to observations at rough coral reefs and breakwaters. It appears that the primary reflector is the shoreline and not scattering by the rough subaqueous bottom. Wave dissipation plays a larger role than wave reflection at this rocky shoreline, which may influence biological community structures and nutrient transport.

THIS PAGE INTENTIONALLY LEFT BLANK

TABLE OF CONTENTS

THIS PAGE INTENTIONALLY LEFT BLANK

LIST OF FIGURES

THIS PAGE INTENTIONALLY LEFT BLANK

LIST OF ACRONYMS AND ABBREVIATIONS

ADCP	Acoustic Doppler Current Profiler
$ADCP_s$	Acoustic Doppler Current Profiler used in shallow deployment (1)
$ADCP_d$	Acoustic Doppler Current Profiler used in deep deployment (2)
AST	Acoustic Surface Tracking
CSUMB	California State University at Monterey Bay
C	Mean Depth-Averaged Wave Speed
D	Distance From Sensor to Reflector
E_{on}	Onshore Directed Wave Energy
E_{off}	Offshore Directed Wave Energy
h	*Depth*
H	*Wave Height*
Hz	Hertz
L	Time Lag in Regard to Determination of Phase-Locking
m	Meter
MSL	Mean Sea Level
Non-PL	Non-Phase-Locked
PL	Phase-Locked
R^2	Wave Energy Reflection Coefficient
S	Spectral Window Length
s	Seconds (time)
SFML	Sea Floor Mapping Laboratory
SNR	Signal to Noise Ratio
T	Period
Δf	Frequency Resolution
η	Sea Surface Elevation
θ	Angle of Wave Direction

THIS PAGE INTENTIONALLY LEFT BLANK

ACKNOWLEDGMENTS

A hearty thanks to my advisor, Jamie MacMahan, for his drive and guidance on this and all my other theses, and allowing me to do so much incredible field work.

Ed Thornton, for his sincere interest and passion, and for providing incredible support on critical ideas and equation development. It was a pleasure.

Lucero Dorantes, for handling this crazy office and starting this project. Your work gave us an amazing launch pad to do some great science.

Casey Gon, for getting out there in the field with me, getting me through it all, and putting my other data to good use.

Dr. Mark Denny and all the staff at Hopkins Marine Lab. It was a privilege to contribute anything to the understanding of such an incredible environment.

Patty Ford, my amazing wife, for everything.

THIS PAGE INTENTIONALLY LEFT BLANK

I. INTRODUCTION

Wave dynamics on rocky shorelines are important for driving currents, inducing large impact velocities on the biological communities that adhere to rock, and providing mixing and exchange that transport nutrients and affect biological recruitment (Denny et al., 2003). Approximately 75% percent of the world's coasts are described as rocky shorelines (Bird, 2000), but the majority of research has been performed on rocky platforms, which comprise only ~20% of rocky shorelines. (Kirk, 1977; Emery and Kuhn, 1982; Trenhaile, 2002). A number of rocky shorelines are composed of a combination of "rougher" geologic features including sea cliffs, marine terraces, sea stacks, rocky shallows, and rocky reefs (Davis and Fitzgerald, 2014). Rough rocky reef-like shorelines have more depth-variability than coral reefs or rocky platforms. The rocky relief is composed of random combination of outcrops that can be fully or partially submerged, and are either attached to a shore platform or a geologic feature further offshore (Winter et al., 2017). Rocky shorelines are commonly studied by marine biologists, as their complex bathymetry and topography promote great biodiversity and complex community structures (Denny et al., 1992; Koehl and Powell, 1994; Trowbridge, 2004). Since rocky shorelines make up so much of the world's coasts and harbor such diverse and unique ecological communities, understanding wave mechanics is pivotal to progressing our knowledge of this important environment.

The amount of wave energy, E, that is available at the shoreline is critical in describing the wave-driven response. Wave energy reflection, R^2, is defined as

$$R^2 = \frac{E_{off}}{E_{on}}, \tag{1}$$

which is the ratio of the offshore-directed (E_{off}) to the onshore-directed (E_{on}) wave energy flux (Elgar et al., 1993). An R^2 of 0 (1) indicates no (perfect) wave energy reflection and 100% (0%) wave energy dissipation. An R^2 between 0 and 1 implies partial wave energy reflection and dissipation.

Field observations of R^2 have been collected for various shoreline configurations and subaqueous bathymetric features, including varying beach slopes on natural sandy beaches, beaches with single and multiple sand bars, coastal breakwater structures, coral reefs, and rocky platforms (Elgar et al., 1993; Elgar et al., 2003; Lentz et al., 2016; Poate et al., 2018). R^2 are typically low (< 0.2), including ~0.1 for a sandy beach at Duck, NC, (Elgar et al., 1993), ~0.1, for a porous rock breakwater in Monterey, CA (Dickson et al., 1995), as well as < 0.1 on coral reefs (Monismith et al., 2015; Lentz et al., 2016). R^2 is also dependent on the incoming wave energy and corresponding frequency (Elgar et al., 1994; Dickson et al., 1995).

There are a few exceptions to the trend of low R^2 , which are associated with unique shoreline configurations. In Massachusetts, beaches supporting multiple sand bars spaced at approximately half the wave-length of incoming waves resulted in an R^2 ranging between 0.4 and 0.7 owing to resonant Bragg reflection that occurred during small (<0.1m) wave heights (Elgar et al., 2003). Guza and O'Reilly (2001) suggested R^2 up to 0.7 for the rocky cliffs along the Channel Islands, California, as the nearly vertical cliffs extend directly into 10–20 m of water.

It is hypothesized that R^2 will be low on a rough rocky reef shoreline considering the previous work described above. Here, an experiment is performed to estimate R^2 on a natural rocky reef at Stanford's Hopkins Marine Laboratory in southern Monterey Bay, CA to test the proposed low R^2 hypothesis. Two Acoustic Doppler Current Profilers (ADCPs) were deployed for computing a non-phase-locked R^2 (Huntley and Davidson, 1998) and a phase locked R^2 (Dickson et al.; 1995, Sheremet et al., 2002). R^2 from the two locations will determine whether there is any potential scattering by the bottom or if the majority is by the shoreline. The experimental set-up is discussed in Chapter II. In Chapter III, the methodology for computing Phase Locked (PL) and Non-Phase Locked (Non-PL) R^2 are described. The observed R^2 and frequency dependence are reported in Chapter IV. The influence of tidal elevation, incoming wave energy, and shoreline effects on R^2 are discussed in Chapter V.

II. EXPERIMENT

Wave energy reflection was measured at a rocky shoreline near Stanford's Hopkins Marine Station, Monterey Bay, CA at two different locations at two different times, as only one Nortek Signature 1000 Acoustic Doppler Current Profiler (ADCP) was available. Hopkins Marine Station is located on a small rocky peninsula surrounded by a rocky reef. For the first deployment, referred to as *shallow* and denoted with an *s* subscript, the $ADCP_s$ was placed in approximately 2.5 m depth of water, 6 m seaward of the shoreline for 20 days from 12 October to 01 November, 2018. The $ADCP_s$ deployment describes R^2 where the shoreline is the primary reflector. For the second deployment, referred to as *deep* and denoted with a *d* subscript, the $ADCP_d$ was placed in 9 m depth of water approximately 100 m from the shore for 13 days from 11–24 June, 2019. The $ADCP_d$ was placed just seaward of the rocky reef, and R^2 is potentially associated with the shoreline reflection and/ or scattering off of the rough bottom. For $ADCP_s$, pressure and wave orbital velocities were burst sampled at 2 Hz for 17 min every 1 hr. For $ADCP_d$, pressure, Acoustic Surface Tracking (AST), and wave orbital velocities were burst sampled at 2 Hz for 17 min every 2 hours. The AST provided direct estimates of sea surface elevations that are typically described from pressure measurements. Velocity data were rotated 13.5° from magnetic north to geographic north.

Wave heights for the shallow and deep deployments were 0.3-1.3m and 0.2-1.0 m, respectively. The waves were primarily associated with narrow-banded swell with an energy peak occurring at about 0.1 Hz. The incoming waves were primarily from the North (350°). The tides are mixed, mainly semi-diurnal, where the low-low tide always follows the high-high tide with a tidal range of approximately 2m (Broenkow and Breaker, 2005).

Local bathymetry was acquired in 2015 by the Sea Floor Mapping Laboratory (SFML) at California State University at Monterey Bay. The SFML survey using the Reson Seabat 7125 multibeam echo sounder resulted in a horizontal resolution of 1 meter and a vertical resolution of 0.20 m (Figure 1a). A two-dimensional vertical profile of the bathymetry between $ADCP_d$ and the shoreline was created (Figure 1b) by plotting the mean depth, +/- standard deviation, and maximum and minimum measured bathymetric height

in relation to cross-shore distance for the 100m alongshore swath from the coastline shown in Figure 1a.

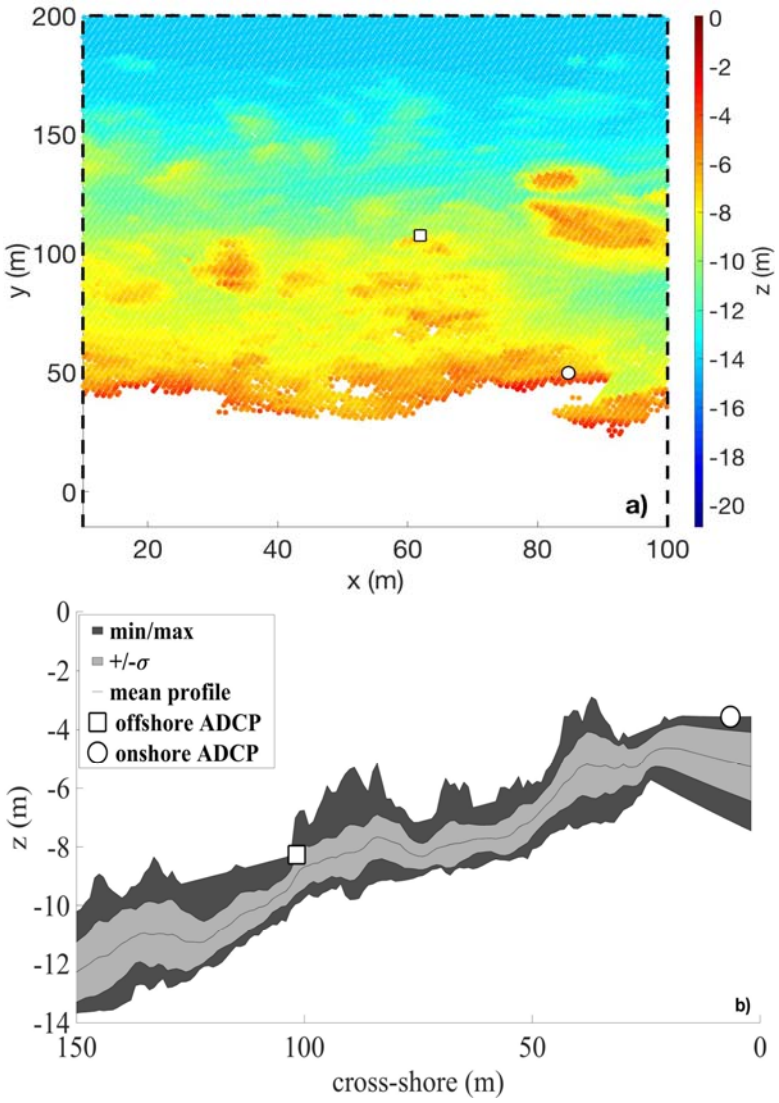

a) Planform of bathymetry for HMS, where the white circle and box denote the locations of the deep and shallow ADCPs. b) Profile of bathymetry, where the black line represents the alongshore mean profile, the light grey area represents one standard deviation from the mean profile, the dark grey area represents the minimum and maximum depths, and the square and circle mark the location of the deep and shallow ADCPs.

Figure 1. a) Planform of bathymetry and b) profile of bathymetry for experiment site

III. METHODS

A. DETERMINATION OF PL AND NON-PL REGIONS

Near a reflective boundary, incoming waves constructively and destructively interact with outgoing reflected waves, forming a (partial) standing wave with nodes (regions of minimum sea surface elevations) and antinodes (regions of maximum sea surface elevations). The region of nodes and antinodes is referred to as Phase-Locked (referred to as *PL*), as described by Huntley and Davidson (1998). Close to the shoreline, the sea surface elevation spectrum has nodes and antinodes that are relatively far apart in frequency. At increasing distance away from the shoreline, the nodes and antinodes become closer in frequency. At a particular distance, the nodes and antinodes overlap in a particular frequency bin together, and the interaction between the ingoing and outgoing waves is reduced and is no longer Phase-Locked (referred to *non-PL*). The determination for whether a region is considered either PL or non-PL is based on the ratio of the non-dispersive time lag, the time interval between the passage of the incoming wave and the return of the reflected wave (defined as L) relative to the length of the spectral window (defined as S) used in computing the energy density spectrum (L/S). L is calculated by

$$L = \left(\frac{d}{C}\right) \times 2, \tag{2}$$

where C is mean depth-averaged wave speed, d is the distance from sensor to the reflector, the coast, in the direction of mean wave propagation. This is multiplied by two to account for time back to the sensor after reflection. When L/S < 0.2, a PL solution that takes into account the interaction between the incoming and reflected waves must be used to accurately estimate the directional wave spectra. When L/S > 0.2, non-PL methods may be used.

The ratio of L/T, where T is the wave period, is used to determine the greatest frequency resolution possible given the window size. As T increases, resolution becomes coarser as less of the wave is captured. For the deep water case, the average wave speed based on the mean depth, C ~6.7m/s, the mean observed wave period was ~7.4s, and window size, S is 100s based on a Δf = 0.01 Hz. With a distance from the sensor to shore

of approximately 100m for the deep deployment, L = 28.7s. The ratios are determined as L/S = 0.287 and L/T = 3.9 for the deep deployment. Following Huntley and Davidson (1998), conditions for the deep deployment allow for the use of Non-PL techniques, with some reduction in resolution. The 6 m distance from the sensor to shore for the shallow deployment results in an L = 1.8s, L/S = 0.018 and L/T = 0.24 for the shallow, recommending the use of PL techniques.

B. WAVE ENERGY REFLECTION METHODS

For the non-PL method, Huntley and Davidson (1998) determined that wave energy reflection, R^2, can be estimated from the directional wave spectrum, $E(f,\theta)$, computed by the Maximum Likelihood Method (MLM) (Capon, 1969; Oltman-Shay and Guza, 1984), described further in Appendix A. The MLM is suggested by Huntley and Davidson (1998) as the first choice of non-PL methods, as it provides high directional resolution without the need for specific spatial information, such as exact location of reflector. The MLM used herein was computed by Nortek's directional wave processing, which optimizes the appropriate depth for the orbital velocities and uses acoustic altimeter for sea surface tracking for sea surface elevation. A spectral hamming window of 100s with 50% overlap was used, resulting in frequency resolution of 0.2Hz and 106 DOF. The directional spectrum was resolved at 4° and smoothed with a 16° degree directional window. Thus, the directional resolution is 16°. The window length and directional resolution are important requirements, as described by Huntley and Davidson (1998).

The computed $E(f,\theta)$ is rotated to account for shoreline orientation (225°), where normally-incident onshore waves are at 0°. Onshore energy is defined between -90° and 90°, and offshore energy is between 90° and -90°, such that

$$E_{on}(f) = \int_{-90}^{90} E(f,\theta)\,d\theta \tag{3}$$

$$E_{off}(f) = \int_{90}^{-90} E(f,\theta)\,d\theta \,. \tag{4}$$

$R^2(f)$ is estimated as (Elgar et al., 2003)

$$R^2\left(f\right)=\frac{E_{off}(f)}{E_{on}(f)}=\frac{\int_{90}^{-90}E(f,\theta)d\theta}{\int_{-90}^{90}E(f,\theta)d\theta}, \tag{5}$$

and the bulk R^2 integrated over frequencies for sea and swell frequencies is

$$R^2=\frac{\int_{0.04}^{0.2}E_{off}(f)}{\int_{0.04}^{0.2}E_{on}(f)}. \tag{6}$$

For the PL region, Huntley and Davidson (1998) suggests the Modified Maximum Likelihood Method (MMLM) (Isobe and Kondo, 1984; Huntley et al., 1995), which incorporates terms accounting for the phase interaction between incoming and reflected waves. This method has two drawbacks: it can produce spurious peaks in the estimated directional spectrum, and requires a distance input from sensor to reflector. ADCPs was so close to the shoreline (6 m) that the change of the shape of the coastline from high to low tide, discussed further in section 5, could potentially produce large errors. R^2 for sea and swell was instead obtained from a modified one-dimensional spectral estimate for a collocated instrument such as an ADCP (Dickson et al., 1995; Sheremet et al., 2002) for a breakwater. It is assumed that the wave angle is small at the shoreline. Burst data were quadratically detrended, divided into 1024s demeaned ensembles. After applying a Hanning window with 50% overlap, cross spectra and spectra were calculated with about 21 degrees of freedom and frequency resolutions of 0.004 Hz. The onshore and offshore energy are estimated by

$$E_{on}(f)=\frac{1}{4}\left(\eta_{pp}+\eta_{uu}+2\eta_{pu}\right)=\frac{1}{4}\left(\frac{Co_{pp}(f,x)}{K_p{}^2}+\frac{Co_{uu}(f,x)}{K_u{}^2}+\frac{Co_{pu}(f,x)}{K_pK_u}\right), \tag{7}$$

$$E_{off}(f)=\frac{1}{4}\left(\eta_{pp}+\eta_{uu}-2\eta_{pp}\right)=\frac{1}{4}\left(\frac{Co_{pp}(f,x)}{K_p{}^2}+\frac{Co_{uu}(f,x)}{K_u{}^2}-\frac{Co_{pu}(f,x)}{K_pK_u}\right), \tag{8}$$

$$K_p=\frac{\cosh k(h+z)}{\cosh(kh)}, \tag{9}$$

$$K_u = 2\pi f \frac{\cosh k(h+z)}{\sinh(kh)}, \tag{10}$$

where C_o is the cospectrum, K_p is the linear wave theory transformation from dynamic pressure to sea surface elevation, K_u is the linear wave theory transformation from cross-shore orbital velocity to sea surface elevation, and subscripts p and u represent dynamic pressure (in decibars) and cross-shore orbital velocity (in m/s), respectively. R^2 is then computed as in Eq. 6. It should be noted that R^2 estimates are sensitive to noise (Huntley et al., 1999; Tatavarti et al., 1995), where the instrument noise has the potential to contaminate and therefore increase R^2, particularly when the signal (incoming waves) are small.

IV. RESULTS

Mean onshore and offshore energy were calculated for the total length of the deep deployment in the sea-swell frequency band (0.05 to 0.2 Hz) and are shown at 0.01Hz intervals in Figure 2a. The onshore and offshore energy is narrow-banded and reaches a maximum of ~2.9 m^2Hz^{-1} at 0.11Hz. The mean R^2_d is variable across frequency, ranging from 0.08 to 0.52, with the lowest R^2_d along the frequency with the largest spectral energy (Figure 2b). It is believed that noise is contributing to higher R^2 for frequencies with lower spectral energy.

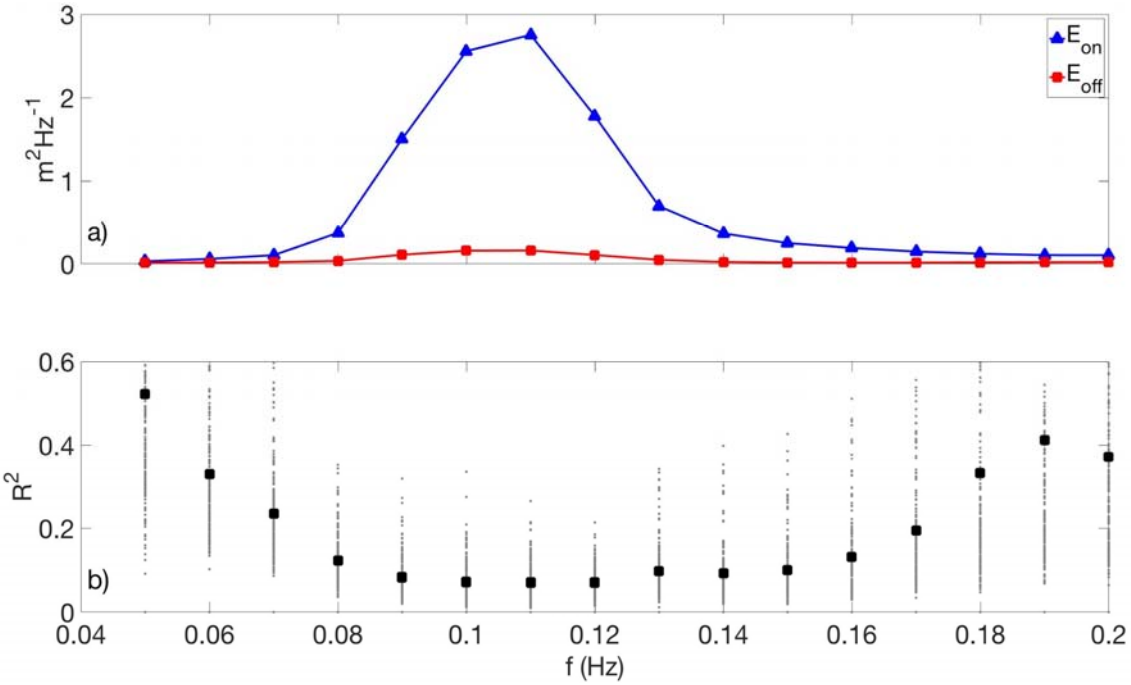

a) Onshore (blue triangles) and offshore (red squares) mean (for all days) energy as a function of frequency at $ADCP_d$. b) R^2 as a function of frequency, where small, grey circles represent the R^2 distribution and large, black squares represent the mean R^2 at each frequency..

Figure 2. a) Offshore and onshore energy and b) R^2 distribution as a function of frequency

A histogram of the fraction of occurrences of bulk R^2 values from the shallow (R^2_s) and deep (R^2_d) deployments shows the majority of R^2 occurrences are clustered between 0.05 and 0.11 (Figure 3). Approximately 80% of R^2_s are between 0.05 and 0.12, while R^2_d has a wider spread, with slightly more occurrences of higher R^2 between 0.13 and 0.21. The mean of these occurrences yields R^2_d ~0.084 +/- 0.006 and R^2_s ~0.079 +/- 0.004 . These low numbers indicate the hypothesis of low R^2 is correct and suggests that the coastline is the primary reflector and the possibility of bottom scattering and resonant Bragg bottom scattering is minimal.

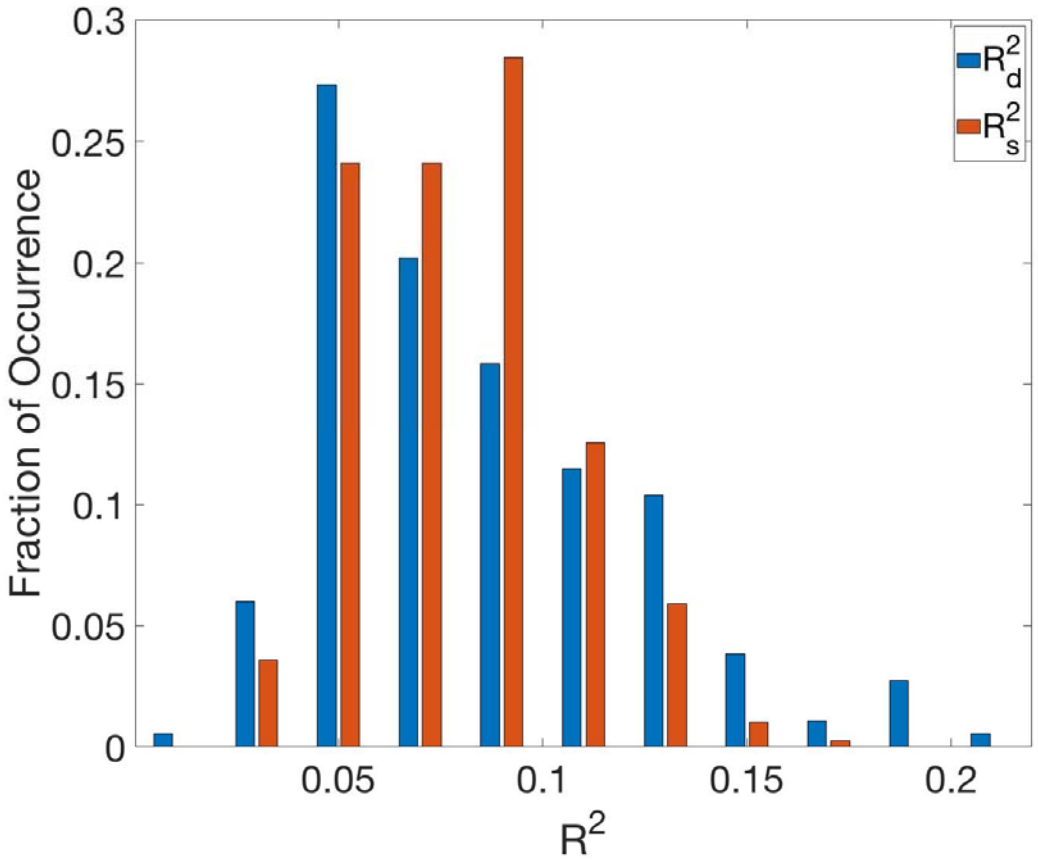

Figure 3. Normalized histogram of fraction of occurrence of bulk R^2_d in blue and R^2_s in red

V. DISCUSSION

A. TIDAL AND ONSHORE ENERGY FLUX INFLUENCE

As low tide rises from -1 to -0.5m, there is no significant difference between the R^2_d, while R^2_s increases very slightly (0.86 to 1.01). During the transition from low to high tide (-0.5 to 0.8m), R_d^2 decreases by ~0.06, and R^2_s by ~0.04, indicating a statistically significant value change between higher tide and decreased R^2 that is small in regards to absolute dynamics but represents a large percent change (Figure 4a,c). Tidal influences are returned to as a factor in the directional spread of reflection, discussed further below. There is a similarly small absolute but large percent decrease of ~0.04 in R_d^2 and ~0.05 in R^2_s as onshore wave energy increases (Figure 4b,d). The decrease in R^2 with increasing energy is surmised to be a result of increased dissipation of breaking wave energy that decreases the percent of outgoing energy.

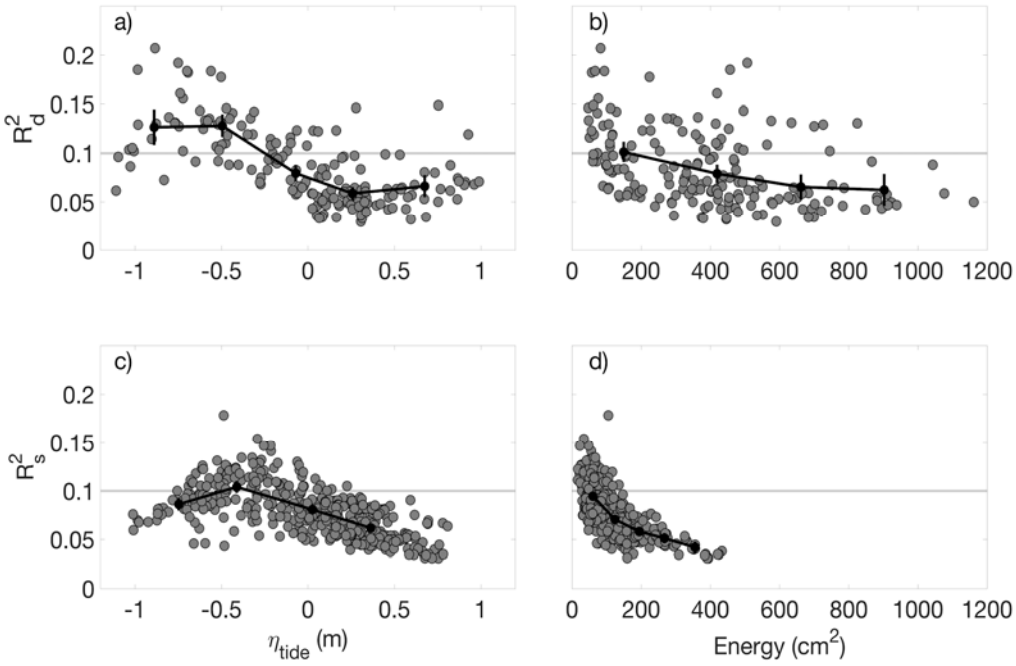

a) R^2 observed during deep deployment (R^2_d) as a function of tide, where grey circles represent the R^2_d distribution, black circles are bin-averaged values of R^2_d, vertical lines at each bin-averaged value are confidence intervals, and grey line is R^2d of 0.1 for use in orientation. b) R^2_d as a function of onshore energy, following the same symbols as a). c) R^2 observed during shallow deployment (R^2_s) as a function of tide, following the same symbols as a) d) R^2_s as a function of onshore energy.

Figure 4. R^2 as a function of tide and onshore energy at both deployment locations

B. SHORELINE ORIENTATION AND ROUGHNESS

In order to numerically calculate R^2, an estimated constant shoreline orientation of 225° has been used. However, a defining characteristic of rocky shorelines is the complex topography, sudden bathymetric changes, and complex network of surge channels that make up the shoreline. Previous studies of reflection involving tides have focused on change in the magnitude of R^2 (Elgar et al., 1993; Guza and O'Reilly, 2001), but the effect on the direction of reflection has not been observed or discussed. The mean observed onshore and offshore angles of $E(f,\theta)$ are 17°and -20°, respectively, which is roughly equal and opposite, or specular. However, the spread of angles is significantly larger, at

16° onshore compared to 45° offshore . Studies of natural sandy beaches observed a significantly smaller spread of offshore energy, ~20° (Elgar et al., 1993). The uniformity of mean values but spread of reflected wave energy directions indicates the general directional roughness of the coast is not the cause of the spreading. The driver of spreading is speculated to be the potentially large changes to the structure of the shoreline with tides, including orientation of the coast and shape of the beach slope. Adding tides to the analysis reveals a weakly correlated but visible trend where the majority of observed reflected wave directions at low tides ($\eta < -0.5$m) are at the extreme low end of the range (0-15°), with only a few outliers just above the mean (Figure 5). High tides ($\eta > 0.5$m) show a similar, though less tightly grouped bias (25 - 45°), all at or above the mean. Such grouping indicates the mean orientation of the shoreline or last few meters of beach slope may be tidally altered.

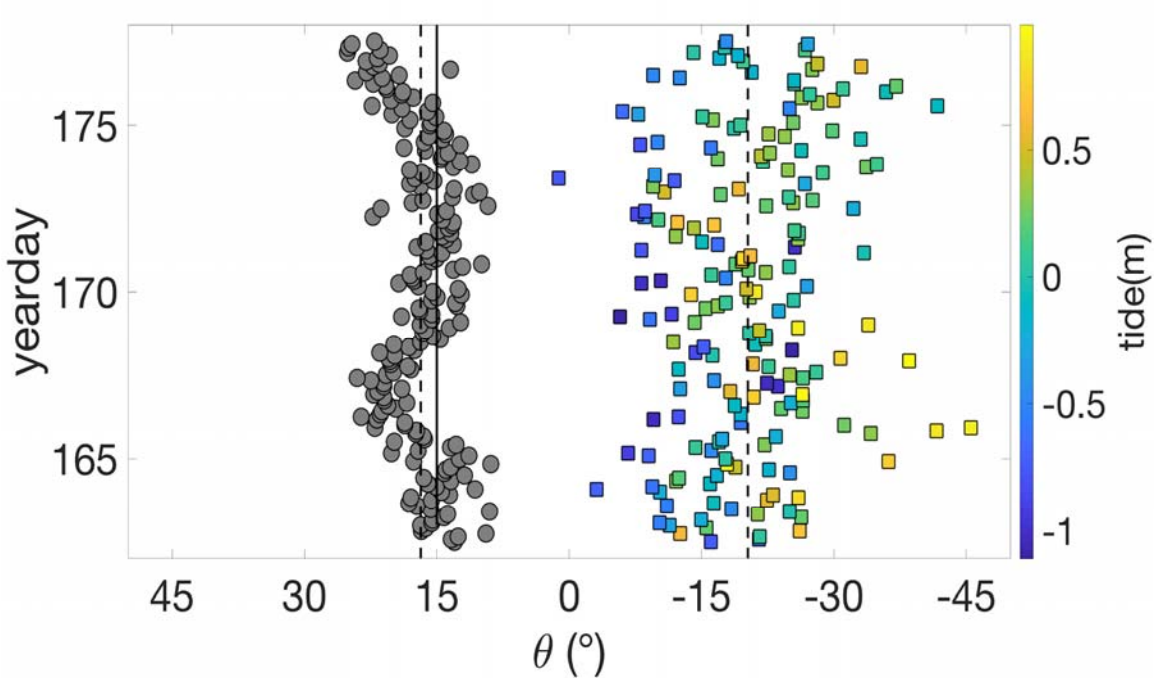

Onshore and offshore propagation angles over time, where grey circles indicate onshore angles, and colored squares indicate offshore angles, where colors follow tide. The dashed line to the left represents the mean onshore angle, and the dashed line to the right represents the mean offshore angle. Solid line represents waves from the NW.

Figure 5. Angular direction of onshore and offshore wave energy with tide

Multiple satellite images provided by Google Earth at high and low tides were examined and a representative estimated shorelines were created to highlight the variability of the coastline with tide (Figure 6). The approximate area of reflection was estimated by applying the observed mean of offshore wave energy backwards from the $ADCP_d$ to the coast, and the mean direction of onshore waves observed at the sensor was extrapolated to the point at the edge of the reef that the angles indicate, based on the observations that oncoming waves were generally uniform offshore.

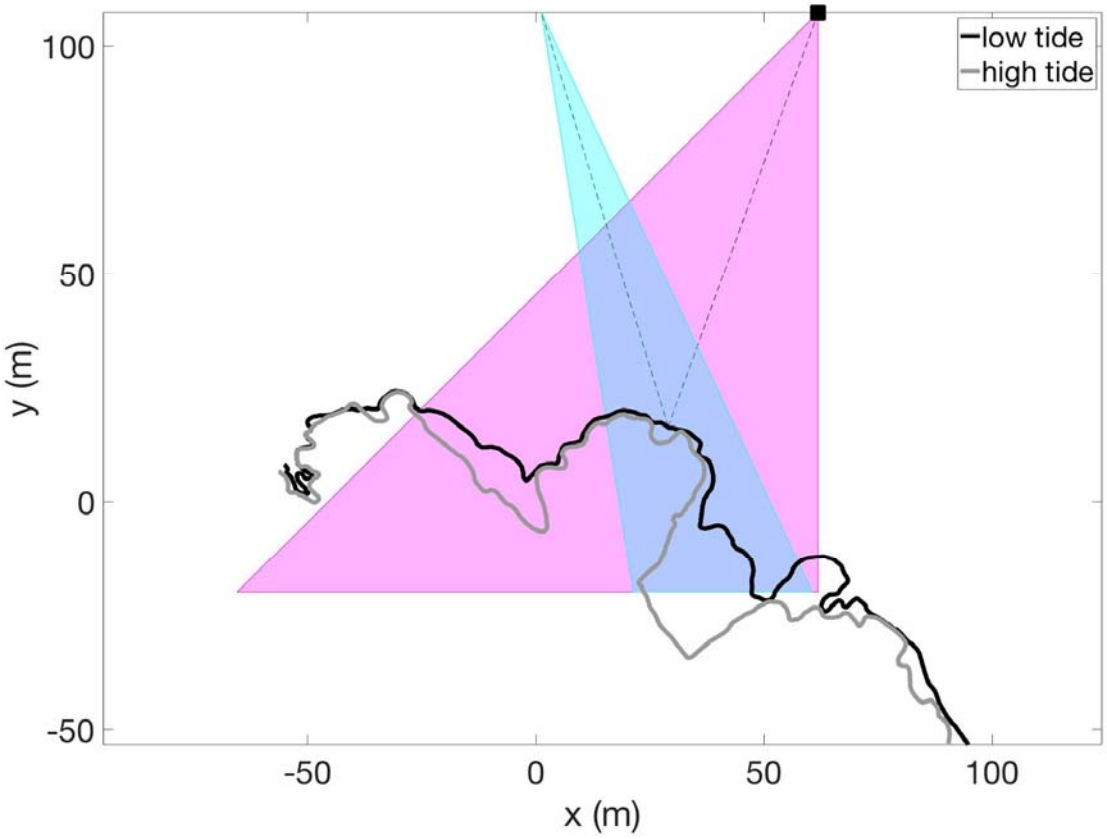

Estimated shorelines at high tide (gray) and low tide (black). Mean angle of incoming and off-going waves indicated by dotted lines with spread and scattering indicated by cyan for incoming waves and magenta cone for off-going.

Figure 6. Estimated shorelines at high and low tide with mean angle and spread and scattering of incoming and off going waves

A significant change in the shoreline occurs between high and low tide, likely due to large sea stacks, boulders, and erosional platforms that become submerged at high tide and erosional platforms that extend the shore at low tide. If oncoming wave energy is uniform, the $ADCP_d$ is observing reflected waves from different sections of the observed coastline during high and low tides. The autocorrelation of the shape of the coastline at high and low tide with x position as the lag value is shown in Figure 7. The e-folding scale occurs at approximately the 20m spatial lag, supporting the visual perception that the coastlines are significantly decorrelated for larger distances.

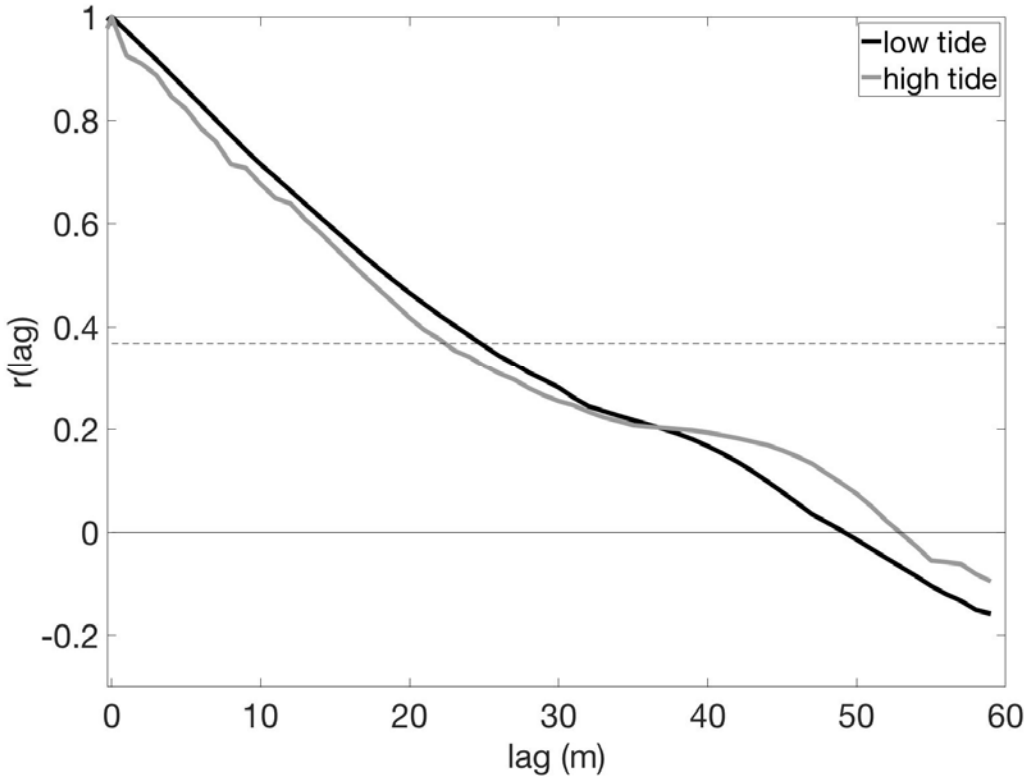

Auto-correlation of roughness at high (gray line) and low (black line) tides. Zero crossing and E-folding are indicated by solid grey and dashed grey line, respectively.

Figure 7. Auto-correlation of coastline roughness at high and low tides with zero crossing and e-folding

C. SCATTERING AND RESONANT BRAGG REFLECTION

As discussed in the introduction, amplification of R^2 to atypically high values (0.7) through resonant Bragg reflection on multiple sandbars was observed at a beach near Truro, Massachusetts (Elgar et al., 2003). These values occurred under very specific conditions: very low (H_{rms}< 0.1m) significant wave heights, and the 50m spacing between the sandbars that was one half the mean wavelength of the incoming waves. R^2 shoreward of the sandbars was 0.4, and 0.7 seaward, indicating amplification occurred due to resonant Bragg reflection processes within the sandbars. The lowest wave heights for the experiment conducted herein were 0.3m, and spacing of the largest rocks in the reef were not even nor one half the wavelength of incoming waves, thus it seemed unlikely that resonant Bragg reflection was occurring at Hopkins Marine Station. To eliminate this possibility, verify that normal reflection or scattering prior on the rocky reef prior to shoreline was not occurring, and determine that the coastline was the primary reflector, R^2_d and R^2_s were compared. Since R^2_s was not significantly smaller than R^2_d and were roughly equal, it is likely that the shore is the primary reflector and scattering amplification by the reef is not a factor in wave reflection. The rocky reef seems to primarily induce dissipation rather than scattering reflection, which agrees with previous results at the site (Gon, 2019).

D. WAVE ENERGY DISSIPATION BY ROUGHNESS

R^2_d and R^2_s being roughly equal introduces a source of confusion in regards to wave transformation and dissipation. A previous study has determined approximately 36% of wave energy dissipation is due to bottom friction of the rocky reef (Gon, 2019). This should result in a decrease of E_{off} as it moves offshore, resulting in R^2_d being smaller than R^2_s. That this is not seen in this experiment is likely related to the shallow deployment location. The only feasible close to shore deployment location was in the vicinity of a channel and not directly in line with the mean direction of onshore wave propagation, which could introduce error related to wave transformation and along shore velocities. Because the bathymetry is so variable at the rocky coast, waves that reach the shallow sensor may not experience the same dissipation as those that pass and return to the deep ADCP. The location of the shallow ADCP near a channel has the potential to introduce higher than

anticipated along-shore velocities and may smear E_{on} into E_{off} in the 1-dimensional assumption used to calculate R^2_s. Taking into account significant error, up to 36% change in E_{off} consistent with Gon (2019), R^2_s would only increase to 0.1 or decrease to 0.06. Neither of these would invalidate the overall finding of low R^2 on a rocky shoreline or indicate a significant enough difference between shallow and deep to suggest resonant Bragg reflection is occurring. There is high confidence in the method used to compute the directional spectrum used in computing R^2_d.

THIS PAGE INTENTIONALLY LEFT BLANK

VI. CONCLUSIONS

The reflection of sea-swell waves from a rocky coast was observed in two deployments using an Acoustic Doppler Current Profiler (ADCP) in 2.5 m depth about 6m from the shore and 9 m depth 100 m offshore at Hopkins Marine Station of Stanford University in southern Monterey Bay. The ratio of offshore to onshore energy spectrally averaged to obtain a bulk R^2, was ~0.08 in both locations. R^2 was compared to tide and onshore energy magnitude. R^2 decreased by 0.05 during the transition from low to high tide, which is a small absolute change, but a large percentage decrease.

The low R^2 suggests that the increased roughness and bathymetric variability of a rocky reef leads to dissipation being the primary dynamic factor for sea-swell wave energy on a rough rocky reef coastline, negating the potential reflective increase that might be expected from a coast made up of large, hard and rough objects. Finding the same R^2 in both locations diverges with previous findings of dissipation with roughness on a rocky reef, and is likely due to directional error associated with 1-dimensional method for the shallow deployment in the vicinity of a channel mouth. Error associated with this does not alter the overall conclusions of this experiment.

The mean wave direction on-shore and off-shore were observed to be approximately equal and opposite (17° and -20°) despite the roughness of the coast, indicating that the mean reflected wave behavior is more dependent on shoreline orientation than roughness. The reflected off-shore wave energy did display a significantly larger spread of 45° that is weakly correlated with tide, in contrast to the narrower spread of 16° of on-shore angles, implying that the shape of a rough, rocky shoreline can be significantly altered by tides. Accounting for the scattering and overall low amount of reflection can lead to new explanations with respect to defining spatial occurrence and conditions of biological communities that live on rocky reefs and potential for new modeling applications or parameterizations for rocky coastlines.

THIS PAGE INTENTIONALLY LEFT BLANK

APPENDIX. MAXIMUM LIKELIHOOD METHOD

For the deep deployment, the general MLM method developed for a pitch and roll buoy (Capon, 1969; Oltman-Shay and Guza, 1984) was followed for use of co-located pressure and horizontal velocity sensor (i.e., Nortek Signature 1000 ADCP). C_{nm} and Q_{nm} are the elements of the normalized cross-spectral matrix of the sea surface elevation and velocities, Φ_{nm}, where

$$\Phi_{nm} = C_{nm} + iQ_{nm}, C_{nm} = C_{nm}^{*} \quad for\, n \neq m. \tag{11}$$

Utilizing the MLM amplitude estimate from Capon et al. (1964), and viewing the wave field as a single plane wave of variance E(α) allows variance at angle α to be estimated as

$$\hat{E}(\alpha) = \sum_{n=1}^{3}\sum_{m=1}^{3} w_n(\alpha) w_m^{*}(\alpha) \Phi_{nm} = E(\alpha) W(\alpha,\alpha) + \int_{0}^{2\pi} W(\alpha,\theta) E_n(\theta)\, d\theta, \tag{12}$$

where $\boldsymbol{\Phi_{nm}}$ is the (n,m) component of the conjugate cross spectrum and has the form

$$\Phi_{nm} = \int_{0}^{2x} E(\theta) G_n(\theta) G_m^{*}(\theta)\, d\theta \tag{13}$$

$$G_1 = 1$$

$$G_2 = i\cos(\theta)$$

$$G_3 = i\sin(\theta).$$

$W(\alpha,\theta)$ is the window function of the form,

$$W(\alpha,\theta) = \sum_{n=1}^{3}\sum_{m=1}^{3} w_n(\alpha) w_m^{*}(\alpha) G_n(\theta) G_m^{*}(\theta) \Phi_{nm} = E(\alpha) W(\alpha,\alpha) + \int_{0}^{2\pi} W(\alpha,\theta) E_n(\theta)\, d\theta \quad . \tag{14}$$

After substituting in the values of $G_n(\theta)$ and imposing a constraint of unity gain on the signal in the absence of noise so that

$$W(\alpha,\theta) = \left| w_1(\alpha) + iw_2(\alpha)\cos(\theta) + iw_n(\alpha)\sin(\alpha) \right| = 1, \tag{15}$$

the variance estimate becomes

$$\widehat{E}(\alpha) = E(\alpha) + \int_0^{2x} W(\alpha,) E_n(\theta)\, d\theta, \tag{16}$$

which is the maximum likelihood estimate. By minimizing the convolution of $\boldsymbol{W(\alpha, \theta)}$and $E_n(\theta)$ and subjecting the minimization to the above constraint, the final form of the estimator is reached:

$$E(f,\theta) = \left\{ \sum_{n=1}^{3} \sum_{m=1}^{3} \Phi_{nm}^{-1} G_n(f,\theta) G_m^*(f,\theta) \right\}^{-1}. \tag{17}$$

The notation is shifted to discuss the directional spectrum of all energy, using the summation of all angles (1-360°)

$$\sum_{\alpha=1}^{360^\circ} \widehat{E}(\alpha) = E(f,\theta) d\theta. \tag{18}$$

LIST OF REFERENCES

Bird, E., 2000: *Coastal Geomorphology: An Introduction*. John Wiley & Sons, 436 pp.

Capon, J., 1969: High resolution frequency-wave-number spectrum analysis. *Proc. IEEE 57,* 1408–1418.

Davis Jr., R. A., & Fitzgerald, D. M., 2004: *Beaches and coasts*. Malden, MA: Blackwell Science Ltd, 419 pp.

Denny, M., J. Dairiki, and S. Distefano, 1992: Biological consequences of topography on wave-swept rocky shores: I. Enhancement of external fertilization. *The Biological Bulletin*, 183, 220–232, https://doi.org/10.2307/1542209.

Denny, M. W., L. P. Miller, M. D. Stokes, L. J. H. Hunt, and B. S. T. Helmuth, 2003: Extreme water velocities: Topographical amplification of wave-induced flow in the surf zone of rocky shores. *Limnology and Oceanography,* 48, 1–8, https://doi.org/10.4319/lo.2003.48.1.0001.

Dickson, W. S., T. H. C. Herbers, and E. B. Thornton, 1995: Wave reflection from breakwater. *Journal of Waterway, Port, Coastal, and Ocean Engineering*, 121, 262–268, https://doi.org/10.1061/(asce)0733-950x(1995)121:5(262).

Elgar, S., Herbers, T. H., & Guza, R. T., 1993: Reflection of ocean surface gravity waves from a natural beach. *Journal of Physical Oceanography*, *24*(7), 1503–1511. doi:10.1175/1520-0485(1994)024<1503:ROOSGW>2.0.CO;2.

Elgar, S., Raubenheimer, B., & Herbers, T. H., 2003: Bragg reflection of ocean waves from sandbars. *Geophysical Research Letters*, *30*(1), 16:1-4, doi:10.1029/ 2002GL016351

Emery, K. O., and G. G. Kuhn, 1982: Sea cliffs: Their processes, profiles, and classification. *Geological Society of America Bulletin*, 93, 644, https://doi.org/ 10.1130/0016-7606(1982)93<644:sctppa>2.0.co;2.

Gon, Casey J, 2019: Wave Transformation on a Rocky Shoreline, Ph.D. Dissertation, Dept. of Oceanography, NPS, Monterey, CA, USA, 2019. [Online]. Available: https://calhoun.nps.edu/handle/10945/63454

Guza , R. and O'Reilly, W., 2001: *Wave Prediction in the Santa Barbara Channel*. MMS OCS Study 2001-055. Coastal Research Center, Marine Science Institute, University of California, Santa Barbara, California. MMS Cooperative Agreement Number 14–35-0001-30758, 8 pp.

Huntley, D. A., Simmonds, D. J., and Davidson, M. A., 1995: Estimation of frequency-dependent reflection coefficients using current and elevation sensors. *Proc., Coast. Dyn.* '95, ASCE, New York, 57–68.

Huntley, D. A., & Davidson, M. A., 1998: Estimating the directional spectrum of waves near a reflector. *Journal of Waterway Port Coastal and Ocean Engineering-ASCE*, *124*(6), 312–319. doi:10.1061/(ASCE)0733-950X(1998)124:6(312).

Huntley, D.A.; Simmonds, D., and Tatavarti, R., 1999. Use of collocated sensors to measure coastal wave reflection. *Journal of Waterway, Port, Coastal, and Ocean Engineering*, 125(1), 46–52.

Huang, W., Chou, C., & Yim, J. Z., 2003: Experiments on the reflection coefficients of a detached breakwater in a directional wave field. *Coastal Engineering*, *47*(4), 367–379. doi:10.1016/S0378-3839(02)00129-1.

Isobe and Kondo, 1984: Methods for estimating directional wave spectra in incident and reflected wave field. *Proc. 19th Conference Coastal Engineering*, ASCE, New York, 467–483.

Kirk, R. M., 1977: Rates and forms of erosion on intertidal platforms at Kaikoura Peninsula, South Island, New Zealand. *New Zealand Journal of Geology and Geophysics*, *20*(3), 571–613. doi:10.1080/00288306.1977.10427603.

Koehl, M. A. R., and Thomas M. Powell, 1994: Turbulent transport of larvae near wave-swept rocky shores: does water motion overwhelm larval sinking. *Reproduction and development of marine invertebrates. Johns Hopkins University Press, Baltimore* : 261–274.

Lentz, S. J., Churchill, J. H., Davis, K. A., Farrar, J. T., Pineda, J., & Starczak, V., 2016: The characteristics and dynamics of wave-driven flow across a platform coral reef in the Red Sea. *Journal of Geophysical Research: Oceans*, *121*(2), 1360–1376. doi:10.1002/2015jc011141.

Monismith, S. G., Rogers, J. S., Koweek, D., & Dunbar, R. B., 2015: Frictional wave dissipation on a remarkably rough reef. *Geophysical Research Letters*, *42*(10), 4063–4071. doi:10.1002/2015gl063804.

Oltman-Shay, J., and R. T. Guza, 1984: A data-adaptive ocean wave directional-spectrum estimator for pitch and roll type measurements. *Journal of Physical Oceanography*, 14, 1800–1810, doi:10.1175/ 1520–0485(1984)014,1800:ADAOWD.2.0.CO;2.

Poate, T., Masselink, G., Austin, M. J., Dickson, M., & McCall, R., 2018: The role of bed roughness in wave transformation across sloping rock shore platforms. *Journal of Geophysical Research: Earth Surface*, *123*(1), 97–123. doi:10.1002/ 2017JF004277

Sheremet, A., Guza, R.T., Elgar, S., Herbers, T.H.C., 2002. Observations of nearshore infragravity waves: seaward and shoreward propagating components. *J. Geophys. Res*. 107. https://doi.org/10.1029/2001JC000970.C8.

Tatavarti, R. V. S. N., Huntley, D. A., and Bowen, A. J., 1988. Incoming and outgoing wave interactions on beaches. *Proc., 21st Conf. on Coast. Engrg., ASCE*, New York, 136–150.

Trenhaile, A. S., 2002: Rock coasts, with particular emphasis on shore platforms. *Geomorphology*, *48*(1-3), 7–22. doi:10.1016/s0169-555x(02)00173-3..

Trowbridge, C. D., 2004: Emerging associations on marine rocky shores: specialist herbivores on introduced macroalgae. *Journal of Animal Ecology*, *73*(2), 294–308, doi:10.1111/j.0021-8790.2004.00808.x.

Winter, G., Lowe, R. J., Symonds, G., Hansen, J. E., & van Dongeren, A. R., 2017: Standing infragravity waves over an alongshore irregular rocky bathymetry. *Journal of Geophysical Research: Oceans*, *122*(6), 4868–4885, doi:10.1002/2016JC012242.

THIS PAGE INTENTIONALLY LEFT BLANK

INITIAL DISTRIBUTION LIST

1. Defense Technical Information Center
   Ft. Belvoir, Virginia

2. Dudley Knox Library
   Naval Postgraduate School
   Monterey, California